

## Resonant tunneling structures based on epitaxial graphene on SiC

This content has been downloaded from IOPscience. Please scroll down to see the full text.

2011 Semicond. Sci. Technol. 26 125012

(<http://iopscience.iop.org/0268-1242/26/12/125012>)

View [the table of contents for this issue](#), or go to the [journal homepage](#) for more

Download details:

IP Address: 128.103.149.52

This content was downloaded on 28/05/2014 at 12:34

Please note that [terms and conditions apply](#).

# Resonant tunneling structures based on epitaxial graphene on SiC

V Hung Nguyen<sup>1,2</sup>, A Bournel<sup>1</sup> and P Dollfus<sup>1</sup>

<sup>1</sup> Institut d'Electronique Fondamentale, UMR8622, CNRS, Université Paris Sud, 91405 Orsay, France

<sup>2</sup> Center for Computational Physics, Institute of Physics, VAST, PO Box 429 Bo Ho, Hanoi 10000, Vietnam

E-mail: [viet-hung.nguyen@u-psud.fr](mailto:viet-hung.nguyen@u-psud.fr)

Received 1 September 2011, in final form 13 October 2011

Published 7 November 2011

Online at [stacks.iop.org/SST/26/125012](http://stacks.iop.org/SST/26/125012)

## Abstract

Recently some experiments have suggested that graphene epitaxially grown on SiC can exhibit an energy bandgap of 260 meV, which enhances the potential of this material for electronic applications. On this basis, we propose to use spatial doping to generate graphene-on-SiC double-barrier structures. The non-equilibrium Green's function technique for solving the massive Dirac model is applied to highlight typical transport phenomena such as the electron confinement and the resonant tunneling effects. The  $I$ - $V$  characteristics of graphene resonant tunneling diodes were then investigated and the effect of different device parameters was discussed. It is finally shown that this kind of double-barrier junction provides an efficient way to confine the charge carriers in graphene and to design graphene resonant tunneling structures.

(Some figures in this article are in colour only in the electronic version)

## 1. Introduction

Graphene and graphene-based nanostructures have recently attracted a great deal of attention for their fascinating fundamental properties and various potential applications [1–4]. This is essentially due to the fact that graphene offers several specific characteristics associated with a zero bandgap electronic structure with chiral massless charge carriers, making it different from conventional solid-state materials. In particular, this material exhibits many unusual transport phenomena such as finite minimal conductivity, unconventional quantum Hall effect or Klein tunneling (see recent reviews [1, 2] and references therein). Besides, due to its exciting properties such as high carrier mobility and small spin-orbit coupling, graphene is expected to be a good candidate for high-speed electronics and spintronics (see [3, 4]).

Different tunneling processes through graphene structures have been discussed in previous works, e.g., see [5–10] or a recent review [11]. In particular, an important transport phenomenon, the resonant tunneling effect, has often been discussed. However, due to the Klein tunneling inherent in massless chiral fermions [5], it was shown to be hard to confine the charges using an external electrostatic potential

in graphene nanostructures [12] and most works have mainly focused on the tunneling processes via hole bound states of the structures. The resonant tunneling processes via electron confined states without the contribution of hole states have recently been discussed in some graphene nanoribbon (GNR) hetero-junctions [13–16], where the confinement is formed owing to discontinuities in the electronic structure between different GNR sections. However, the design of nanoribbon hetero-structures always raises a technological challenge of controlling precisely their width and edges at the atomic scale. The results obtained for such hetero-structures were shown to be very sensitive to the structure designs and to the edge disorder effects [16]. Moreover, GNR devices have limited driving currents, and, therefore, their use for realistic applications requires the production of dense arrays of ordered nanoribbons. In this view, besides better understanding the charge transport in graphene quantum structures, the systematical investigation of the resonant tunneling devices based on 2D gapped graphene sheets is desirable for the development of such materials in electronics.

To confine efficiently the charge carriers in graphene nanostructures, opening a finite energy bandgap is a key point. In fact, it can be achieved not only by patterning a graphene sheet into nanoribbons [17] but also when the inversion

symmetry of the graphene plane is broken as suggested in recent works [18–22]. In particular, the experiment reported in [18] has demonstrated that graphene epitaxially grown on the SiC substrate can exhibit a bandgap of up to 260 meV. Although relatively small compared to that in conventional semiconductors, it is about ten times greater than the thermal energy at room temperature, which has stimulated some studies of 2D graphene in electronics [23–26]. Hence, instead of GNR hetero-junctions [16], we propose here to use a spatial doping to form graphene-on-SiC double-barrier structures. We demonstrate that electron states can be fully confined and strong resonant tunneling effects are achieved in these structures, which are appropriate for designing efficient graphene resonant tunneling diodes (RTDs).

The paper is thus organized as follows. In section 2, the simulated structures and the calculation method are described. The obtained results are presented and discussed in section 3: the confinement of electrons, the resonant tunneling and the negative differential conductance (NDC) effects in subsection 3.1, the influence of main structure parameters, the well thickness, the barrier thickness and the transition length in subsection 3.2. Finally, a conclusion is given in section 4.

## 2. Model and calculation

Graphene has a honeycomb lattice with a unit cell consisting of two carbon atoms—normally referred to as  $A$  and  $B$  atoms. To describe the charge states in the system, a simple nearest-neighbor tight binding model can be conveniently used, with  $a_c = 0.142$  nm the carbon–carbon distance,  $t = 2.7$  eV the hopping energy between nearest-neighbor sites and  $\varepsilon_A = -\varepsilon_B = \Delta$  the on-site energies in the two sublattices. While  $\Delta = 0$  in the pristine sheet, it is finite ( $\approx 130$  meV) when the graphene is epitaxially grown on SiC [18]. Using such a model, the energy dispersion close to the  $\mathbf{K}$ -point can simply be written as

$$E(\vec{k}) = \pm \sqrt{\hbar^2 v_F^2 (k_x^2 + k_y^2) + \Delta^2}, \quad (1)$$

where  $v_F = 3a_c t / 2\hbar \approx 10^6$  m s<sup>-1</sup> is the Fermi velocity,  $\vec{k} = (k_x, k_y)$  is the 2D momentum measured relatively to the  $\mathbf{K}$ -point and the sign  $\pm$  stands for the conduction/valence band, respectively. From equation (1), the bandgap is determined as  $E_G = 2\Delta$  ( $\approx 260$  meV). To consider the charge transport in such a system, one can conveniently use the following massive Dirac-like Hamiltonian:

$$\mathcal{H} = -i\hbar v_F (\sigma_x \partial_x + \sigma_y \partial_y) + \Delta \sigma_z + U(x), \quad (2)$$

where  $U$  is the external potential energy and  $\sigma_{x,y,z}$  are the Pauli matrices. We assume the width of the graphene sheet to be much larger than the length of the active region (e.g. a few tens of nm as in our simulations below) so that the potential energy can be modeled as just a function of  $x$  in this study. This assumption ignores the role of graphene edges and lateral confinement effects which are important for narrow GNR channels.

To solve equation (2), an efficient method has been proposed by rewriting the Hamiltonian within a tight-binding formulation in a new basis  $\{|x_n\rangle, |k_y\rangle\}$ , where  $|k_y\rangle = e^{ik_y y}$

and  $x_{n+1} - x_n = a_0$  is an arbitrary mesh spacing [8, 9, 26]. Throughout the work,  $a_0$  is chosen to be 0.2 nm, which is proved to be small enough to give accurate results. The device-retarded Green's function is then defined as

$$G^r(E, k_y) = [E + i\eta - \mathcal{H} - \Sigma_L - \Sigma_R]^{-1} \quad (3)$$

with the left (right) self-energy  $\Sigma_{L(R)}$ , which describes the device-to-contact coupling. The transmission coefficient needed to define the current and the local density of states (LDOS) are defined as  $T(E, k_y) = \text{Tr}[\Gamma_L G^r \Gamma_R G^{r\dagger}]$  and  $\mathcal{D}(x_n) = -\text{Im}[G_{n,n}^r(E)]/\pi$ , respectively, where  $\Gamma_{L(R)} = i(\Sigma_L - \Sigma_L^\dagger)$ . Finally, the current density is computed by the Landauer formula

$$J = \frac{2e}{\pi h} \int_{-\infty}^{\infty} dE dk_y T [f_L(E) - f_R(E)], \quad (4)$$

where  $f_{L(R)}(E) = 1/[1 + \exp((E - E_{FL(R)})/k_b T)]$  is the Fermi distribution function in the left (right) contact with the Fermi energy  $E_{FL(R)}$ .

The formalism described above is used to investigate the ballistic transport characteristics of graphene double-barrier structures wherein the two potential barriers are formed by a spatial doping, i.e. the npnpn-junctions schematized in figure 1. The doped graphene regions are assumed to be generated by using electrostatic doping [27, 28] or chemical doping [29, 30]. The key structure parameters are the potential barrier  $U_0$ , the barrier thickness  $L$  and the well thickness  $D$  separating the barriers. The doping is known to affect/generate a bandgap in graphene, e.g., see a recent review [31]. Although not taken into account here, this effect provides additional possibilities of bandgap engineering, which may be useful for designing graphene resonant tunneling structures as proposed in this work.

Moreover, as discussed in [26], the charge transport through the junction of different doped zones is very sensitive to the length of the transition region across which the charge density changes monotonically from n-type to p-type. This is essentially due to the fact that an increase in this length enhances the contribution of evanescent states around the neutral points in the transition regions, which reduces the interband tunneling of charges from the n-doped side to the p-doped one. Although the interband tunneling does not play any important role in the structures studied here, the transition length influences the effective barrier and well thicknesses, which may change the confined levels and the resonant tunneling. In the major parts of the paper, the transition length of 1 nm is assumed. The effects of this length (particularly, in the range 1–6 nm) are then discussed in the final part.

## 3. Results and discussion

### 3.1. Electron confinement, resonant tunneling and negative differential conductance effects

In this subsection, we describe how the confinement and the resonant tunneling effects are obtained in double-barrier graphene structures using a spatial doping. In figures 2(a) and (c), we plot the maps of LDOS for  $U_0 = 0.38$  eV  $> E_G$  and

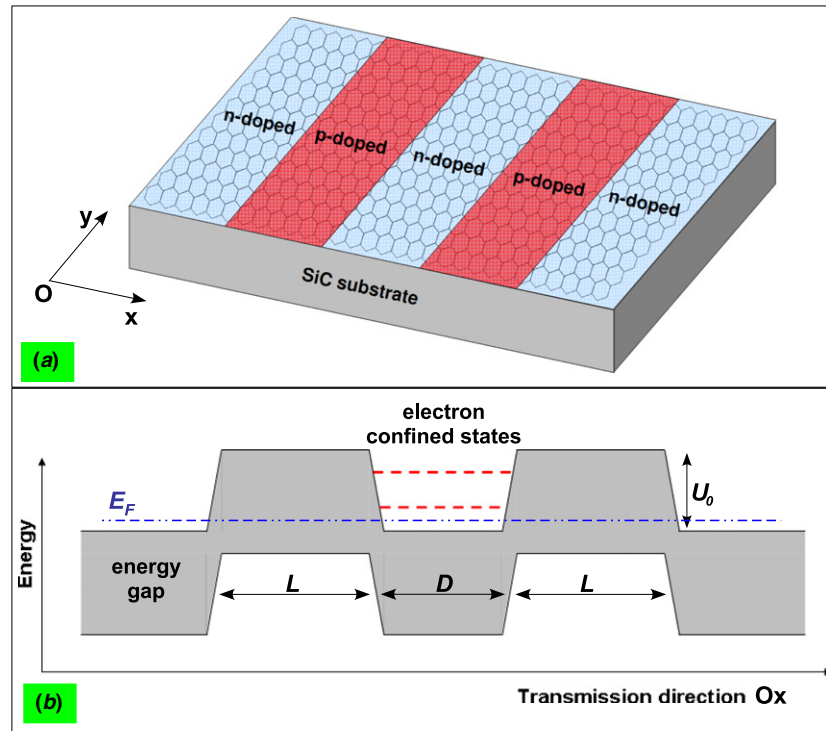


**Figure 1.** (a) Schematic of graphene-on-SiC double-barrier structures formed by a spatial doping and (b) their energy band diagram.

for  $U_0 = E_G = 0.26$  eV, respectively, and for normal incident particles ( $k_y = 0$ ). Besides, the corresponding transmission coefficients are displayed in figures 2(b) and (d) as a function of energy. They exhibit peaks of resonant tunneling through the structure. In both cases, we observe clearly the confined states of electrons in the well region (see figures 2(a) and (c)). For  $U_0 > E_G$ , we even find hole confined states in the barrier regions (figure 2(a)), which are known to govern the Klein tunneling (the transmission peak is plotted in figure 2(b), dashed line) of chiral fermions [8]. As mentioned above, since such a transmission process has been investigated carefully in previous works [7–9], we mainly focus here on the tunneling via the confined electron states. For  $U_0 \leq E_G$  (figures 2(c) and (d)), when the Klein tunneling process is fully suppressed, the confinement and resonant effects are shown to be stronger than those in gapless graphene structures. This is due to the fact that these effects are obtained even for normal incident particles ( $k_y = 0$ ) and weakly  $k_y$  dependent in this study. In contrast, the situation is very different in the case of gapless graphene where the transmission is nearly perfect and almost suppressed for small  $k_y$  in monolayer [7, 8] and bilayer structures [9], respectively, and thus strongly dependent on  $k_y$ . To see more clearly the dependence of the resonant tunneling on  $k_y$ , we display a  $(k_x, k_y)$  contour plot of the transmission coefficient in figure 3. Practically, the slow reduction of the width of the resonant peaks is observed with increasing  $k_y$ . This feature normally appears in all graphene structures and can be explained by the fact that the resonant tunneling is affected by the contribution of evanescent states in the barrier regions which decay with increasing  $k_y$  due to the increase of the effective transmission gap  $\hat{E}_G = 2\sqrt{\Delta^2 + \hbar^2 v_F^2 k_y^2}$ . However, the resonant effects are observed for almost all values of  $k_y$ .

Based on this, it is expected that the effects on the electrical current in the considered structures are stronger than for the gapless graphene ones [7–9].

This idea is now demonstrated in figure 4(a), where we plot the  $I$ – $V$  characteristics of the structure with  $U_0 = 0.26$  eV at different temperatures ranging from 77 K to 300 K. Indeed, a high peak current and a strong NDC effect are observed clearly in all the cases studied. Besides, it is shown that when the temperature is increased from 77 K to 150 K, the smearing effect leads to a decreased peak current and an increased valley one, which finally reduces the peak-to-valley ratio (PVR) of NDC. However, both of them increase when the temperature is raised to 300 K. This behavior can be understood by the contribution of the second confined level (see figure 2(c)). In spite of such smearing effects, it is remarkable to see that a PVR as high as 4.1 is achieved at room temperature. When changing appropriately the device parameters, e.g., increasing the barrier thickness, the room temperature PVR can even reach about 7–8, but at the price of a reduced peak current (discussed later). Such a high PVR is comparable to the best value obtained in the GNR-RTDs [16] and in conventional semiconducting RTDs [32, 33].

To analyze the effects of the Klein tunneling observed in figure 2(b), we display in figure 4(b) the  $I$ – $V$  characteristics obtained for different  $U_0$  at  $T = 77$  K. On increasing  $U_0$  ( $U_0 > E_G$ ), due to the contribution of the transmission peak associated with the Klein tunneling, the overall current increases and two NDC regions can be obtained in the bias range considered 0–0.3 V. However, the large increase in the valley current for  $U_0 = 0.38$  and 0.5 eV finally leads to the PVRs smaller than those in the case of  $U_0 = 0.26$  eV (without the Klein tunneling). For instance, the maximum PVR (i.e.

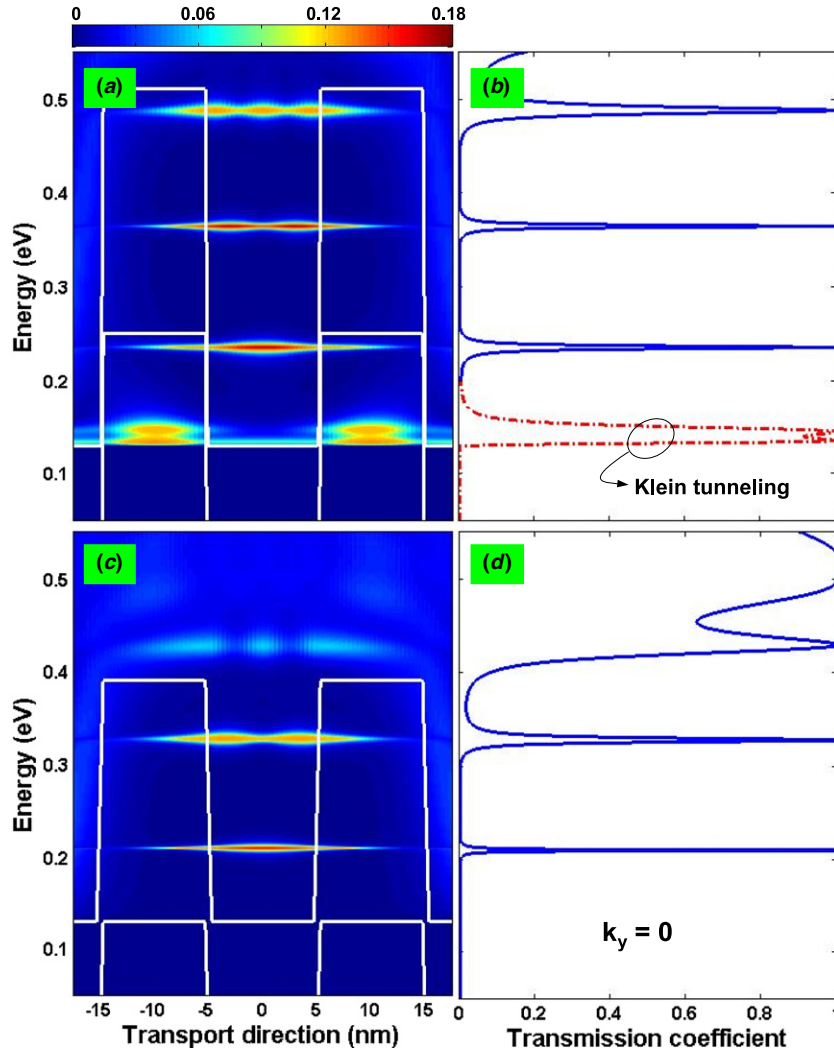


**Figure 2.** (a) and (c) LDOS and (b) and (d) corresponding transmission coefficient as a function of energy in graphene-on-SiC double-barrier structures. The structure parameters are  $L = D = 10$  nm,  $k_y = 0$ ,  $U_0 = 0.38$  eV in (a) and (b) and 0.26 eV in (c) and (d). The white solid line in (a) and (c) shows the bottom of the conduction band and the top of the valence band profiles.

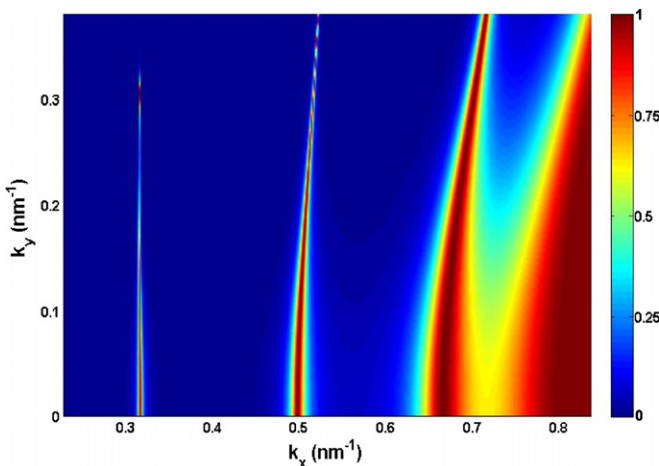


**Figure 3.** The  $(k_x, k_y)$  map of the transmission coefficient through a graphene-on-SiC double-barrier structure. Other parameters are  $L = 8$  nm,  $D = 10$  nm and  $U = 0.26$  eV.

second peak current/second valley current) falls to 65 and 34 for  $U_0 = 0.38$  and 0.5 eV, respectively, while it reaches 94 for

$U_0 = 0.26$  eV. Hence, the Klein tunneling may be exploited to enhance the overall current but it reduces the PVR value.

### 3.2. Influence of well thickness, barrier thickness and transition length

We now discuss the role of two structure parameters, the well and the barrier thicknesses. We first present an  $(E, D)$ -map of the transmission coefficient in figure 5(a). In principle, the bound states in the well region correspond to the quantized values of  $k_x$ , which are defined by  $k_x = n\pi/D$  ( $n$  is an integer) in the case of infinite barriers [34]. In the case of finite barriers studied here, this simple expression describes well only the low-energy confined levels, e.g., the first confined level/resonant peak in figure 3. This feature together with the energy dispersion described in equation (1) explains well the unusual quantization of fermions in graphene structures: the energy spacing between the resonant peaks is nearly proportional to  $1/D$  as may be seen in the evolution of resonant peaks with respect to the thickness  $D$  in figure 5(a), but not

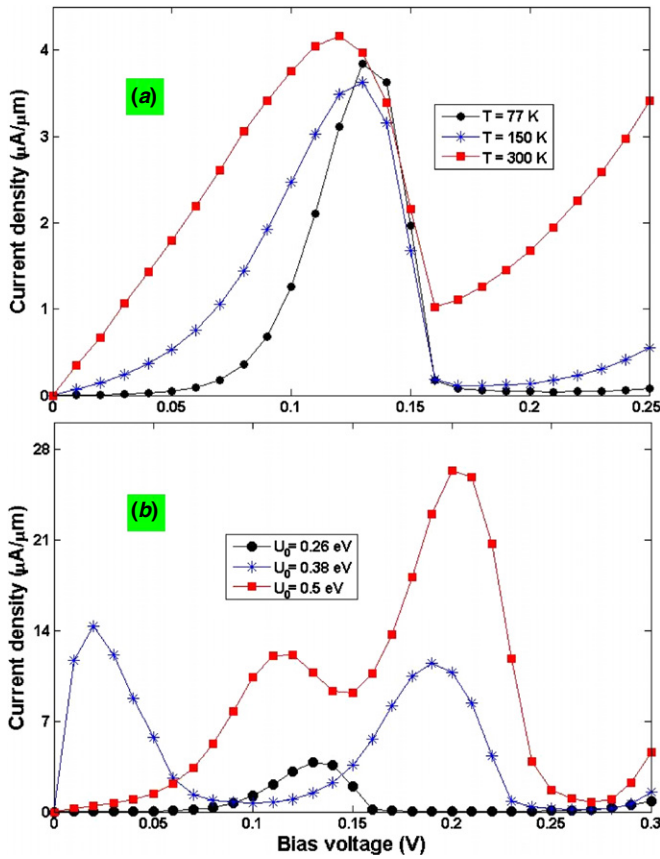


**Figure 4.**  $I$ - $V$  characteristics of graphene-on-SiC RTDs at different temperatures (a) and different barrier heights (b). Unless otherwise stated,  $E_F = 0.15$  eV,  $L = D = 10$  nm,  $U_0 = 0.26$  eV and  $T = 77$  K.

to  $1/D^2$  as in conventional materials [7, 8, 11]. To see the role of the barrier thickness in the tunneling current through the system, we display an  $(E, L)$ -map of the transmission coefficient in figure 5(b). The intensity and width of the resonant peaks are shown to decay with the increase of the

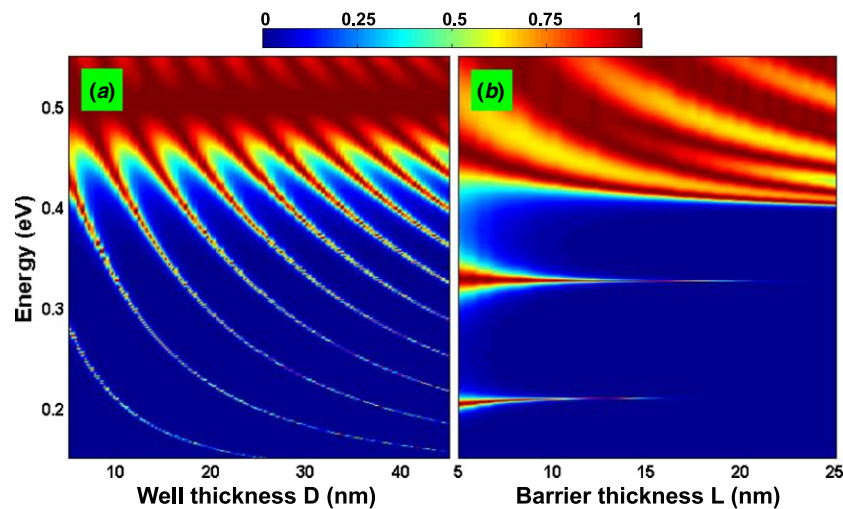


**Figure 5.** (a)  $(E, D)$ - and (b)  $(E, L)$ -maps of the transmission coefficient for  $k_y = 0$ . Other parameters are  $L = 10$  nm in (a),  $D = 10$  nm in (b) and  $U = 0.26$  eV.

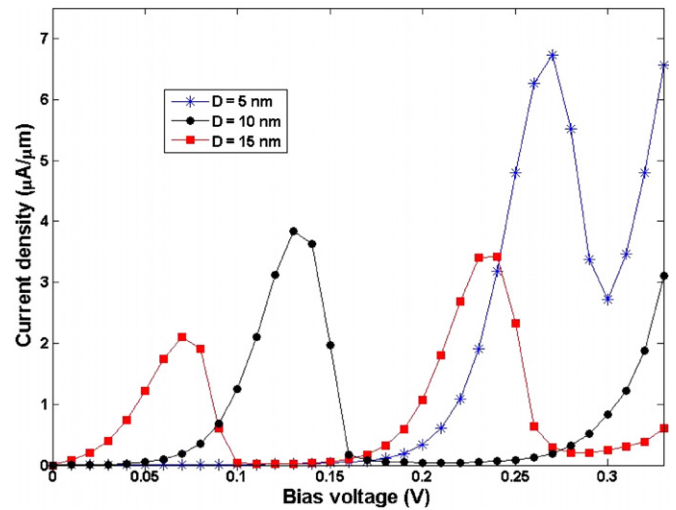


**Figure 6.**  $I$ - $V$  characteristics of graphene-on-SiC RTDs for different well thicknesses. Other structure parameters are  $E_F = 0.15$  eV,  $L = 10$  nm,  $U = 0.26$  eV and  $T = 77$  K.

barrier thickness. This result is explained well by the fact that the tunneling transmission through the barriers is affected strongly by the evanescent states in the barrier regions, whose wavefunctions tend to vanish with increasing  $L$ .

To evaluate the roles of these parameters on the RTD operation, we first display the  $I$ - $V$  characteristics for different well thicknesses in figure 6. Due to the change in the position of confined levels as seen in figure 5(a), the position of the first peak current (similar to that observed in [16]) moves to the low bias with increasing  $D$ . Moreover, the reduction of not only the peak current but also the valley one is observed. The latter feature can be explained by the smaller contribution of the thermionic transmission at low bias, which thus results in an increased PVR in the first NDC region, i.e. it is about 2.5, 94 and 111 for  $D = 5, 10$  and  $15$  nm, respectively. Besides, because the number of resonant peaks increases with respect to  $D$ , the second peak current/NDC behavior can be observed for large  $D$  in the considered bias range (i.e. see the case of

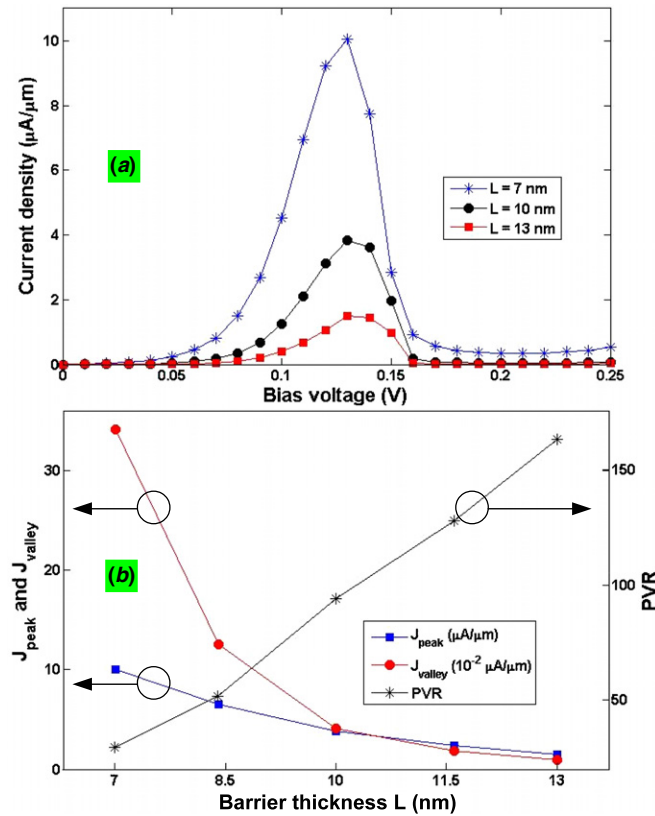


**Figure 7.** (a)  $I$ - $V$  characteristics of graphene-on-SiC RTDs for different barrier thicknesses. (b) The dependence of  $J_{\text{peak}}$ ,  $J_{\text{valley}}$  (left axis) and the PVR (right axis) on  $L$ . Other parameters are  $E_F = 0.15$  eV,  $D = 10$  nm,  $U = 0.26$  eV and  $T = 77$  K.

$D = 15$  nm in figure 6). Next, the  $I$ - $V$  characteristics and the evolution of the peak and the valley currents as a function of  $L$  are displayed in figure 7. Due to the reduction of the resonant tunneling discussed above, both the peak and the valley currents strongly decrease with increasing  $L$ , which results in an increased PVR as seen in figure 7(b). This suggests that a strong NDC effect can be achieved for large barriers but at the price of a small peak current.

Finally, we discuss the role of the transition length  $L_t$  in the transport in the considered structures. In figure 8, the transmission coefficient for  $k_y = 0$  at zero bias and the  $I$ - $V$  characteristics are displayed for different  $L_t$ , while the average thickness of the well and the barrier is unchanged. Figure 8(a) shows that on increasing  $L_t$ , (i) the transmission coefficient at low energy is reduced because of the higher influence of evanescent states in the barrier regions, i.e. the barrier thickness in this energy regime is enlarged; (ii) the resonant peak is shifted to higher energy and its width is simultaneously reduced. These effects of course govern the behaviors of the  $I$ - $V$  characteristics as shown in figure 8(b). On one hand, the current peak is shifted to higher bias, and on the other hand, both its width and height decrease with increasing  $L_t$ . This result finally suggests that a sharp profile is desirable for achieving strong resonant effects, though they remain significant for large  $L_t$ . Such a short transition length (sharp profile) may be realized by controlling the device design, e.g., by appropriately reducing the gate dielectric thickness in the

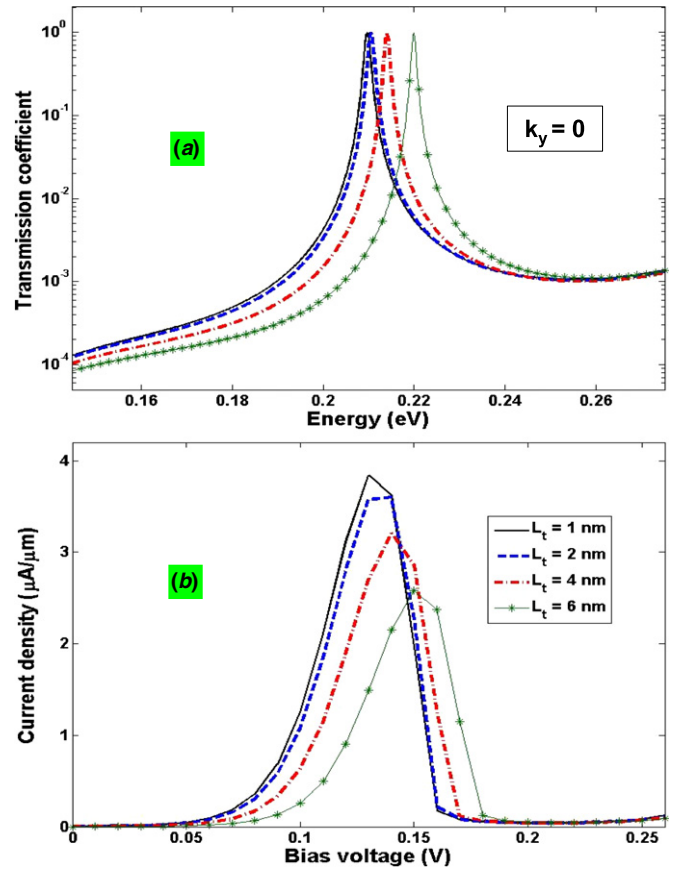


**Figure 8.** (a) Transmission coefficient for  $k_y = 0$  at zero bias and (b)  $I$ - $V$  characteristics of graphene-on-SiC RTDs for different transition lengths  $L_t$ . Other parameters are  $E_F = 0.15$  eV,  $L = D = 10$  nm,  $U = 0.26$  eV and  $T = 77$  K.

case of the electrostatic doping [28], or by using the chemical doping to generate the p-n junctions as mentioned in [29].

#### 4. Conclusion

We have proposed a graphene-on-SiC resonant tunneling structure that can be realized by using a spatial doping. The non-equilibrium Green's function technique was applied to highlight the transport characteristics such as the electron confinement, the resonant tunneling and the negative differential conductance effects in these structures. It was found that due to the suppression of Klein tunneling, the complete confinement of electron states can be achieved and the resonant tunneling effects are strong in comparison with what can be obtained in gapless graphene structures. Therefore, a significant negative differential conductance effect is observed. The roles of main structure parameters, the well thickness, the barrier thickness and the transition length, were then discussed. This study is an additional contribution to our understanding of the different kinds of tunneling processes in 2D graphene structures and may be helpful for further investigations and design of graphene-based quantum structures/electronic devices.

## Acknowledgments

This work was partially supported by the French ANR through the projects NANOSIM-GRAPHENE (ANR-09-NANO-016) and MIGRAQUEL (ANR-10-BLAN-0304). One of the authors (VHN) acknowledges the Vietnam's National Foundation for Science and Technology Development (NAFOSTED) for financial support under the project no 103.02-2010.33.

## References

- [1] Neto A H C, Guinea F, Peres N M R, Novoselov K S and Geim A K 2009 *Rev. Mod. Phys.* **81** 109
- [2] Abergel D S L, Apalkov V, Berashevich J, Ziegler K and Chakraborty T 2010 *Adv. Phys.* **59** 261
- [3] Schwierz F 2010 *Nat. Nanotechnol.* **5** 487
- [4] Yazyev O V 2010 *Rep. Prog. Phys.* **73** 056501
- [5] Katsnelson M I, Novoselov K S and Geim A K 2006 *Nat. Phys.* **2** 620
- [6] Bai C and Zhang X 2007 *Phys. Rev. B* **76** 075430
- [7] Pereira J M Jr, Vasilopoulos P and Peeters F M 2007 *Appl. Phys. Lett.* **90** 132122
- [8] Do Nam V, Nguyen V H, Dollfus P and Bournel A 2008 *J. Appl. Phys.* **104** 063708
- [9] Nguyen V H, Bournel A, Nguyen V L and Dollfus P 2009 *Appl. Phys. Lett.* **95** 232115
- [10] Kundu A, Rao S and Saha A 2010 *Phys. Rev. B* **82** 155441
- [11] Barbier M, Vasilopoulos P and Peeters F M 2010 *Phil. Trans. R. Soc. A* **368** 5499
- [12] Matulis A and Peeters F M 2008 *Phys. Rev. B* **77** 115423
- [13] Blanter Ya M and Martin I 2007 *Phys. Rev. B* **76** 155433
- [14] Zhang Z Z, Chang K and Chan K S 2008 *Appl. Phys. Lett.* **93** 062106
- [15] Zhang Z Z, Wu Z H, Chang K and Peeters F M 2009 *Nanotechnology* **20** 415203
- [16] Teong H, Lam K-T, Khalid S B and Liang G 2009 *J. Appl. Phys.* **105** 084317
- [17] Liang G, Khalid S B and Lam K-T 2010 *J. Phys. D: Appl. Phys.* **43** 215101
- [18] Han M Y, Özyilmaz B, Zhang Y and Kim P 2007 *Phys. Rev. Lett.* **98** 206805
- [19] Zhou S Y, Gweon G-H, Fedorov A V, First P N, de Heer W A, Lee D-H, Guinea F, Neto A H Castro and Lanzara A 2007 *Nat. Mater.* **6** 770
- [20] Vitali L, Riedl C, Ohmann R, Brihuega I, Starke U and Kern K 2008 *Surf. Sci.* **602** L127
- [21] Enderlein C, Kim Y S, Bostwick A, Rotenberg E and Horn K 2010 *New J. Phys.* **12** 033014
- [22] Balog R *et al* 2010 *Nat. Mater.* **9** 315
- [23] Yavari F, Kritzinger C, Gaire C, Song L, Gullapalli H, Borca-Tasciuc T, Ajayan P M and Koratkar N 2010 *Small* **6** 2535
- [24] Kedzierski J, Hsu P-L, Healey P, Wyatt P W, Keast C L, Sprinkle M, Berger C and de Heer W A 2008 *IEEE Trans. Electron Devices* **55** 2078
- [25] Cheli M, Michetti P and Iannaccone G 2010 *IEEE Trans. Electron Devices* **57** 1936
- [26] Michetti P, Cheli M and Iannaccone G 2010 *Appl. Phys. Lett.* **96** 133508
- [27] Nguyen V H, Bournel A and Dollfus P 2011 *J. Appl. Phys.* **109** 093706
- [28] Huard B, Sulpizio J A, Stander N, Todd K, Yang B and Goldhaber-Gordon D 2007 *Phys. Rev. Lett.* **98** 236803
- [29] Zhang L M and Fogler M M 2008 *Phys. Rev. Lett.* **100** 116804
- [30] Low T, Hong S, Appenzeller J, Datta S and Lundstrom M S 2009 *IEEE Trans. Electron Devices* **56** 1292
- [31] Farmer D B, Lin Y-M, Afzali-Ardakani A and Avouris P 2009 *Appl. Phys. Lett.* **94** 213106
- [32] Brenner K and Murali R 2010 *Appl. Phys. Lett.* **96** 063104
- [33] Liu H, Liu Y and Zhu D 2011 *J. Mater. Chem.* **21** 3335
- [34] Mizuta H and Tanoue T 1995 *The Physics and Applications of Resonant Tunneling Diodes* (Cambridge: Cambridge University Press)
- [35] Sun J P, Haddad G I, Mazumder P and Schulman J N 1998 *Proc. IEEE* **86** 641
- [36] Ferry D K and Goodnick S M 2001 *Transport in Nanostructures* (New York: Cambridge University Press)